Supplementary Information:

Graphene/nitrogen-functionalized graphene quantum dots hybrid broadband photodetectors with buffer layer of boron nitride nanosheets

Hiroyuki Tetsuka*, Akihiro Nagoya and Shin-ichi Tamura

Frontier Research-Domain, Toyota Central R&D Labs., Inc., 41-1 Yokomichi, Nagakute, Aichi 480-1192, Japan
E-mail: h-tetsuka@mosk.tytlabs.co.jp

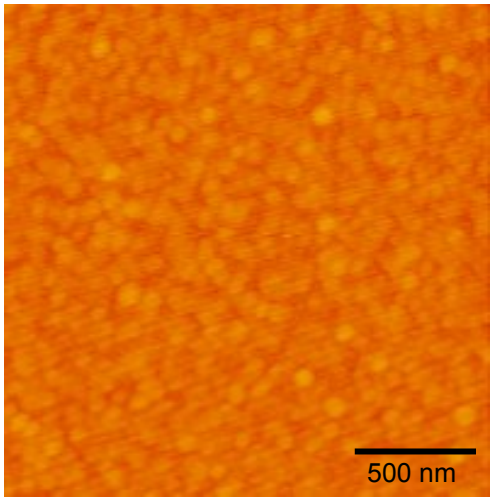

Fig. S1 AFM image of BN-NSs layer coated on graphene.

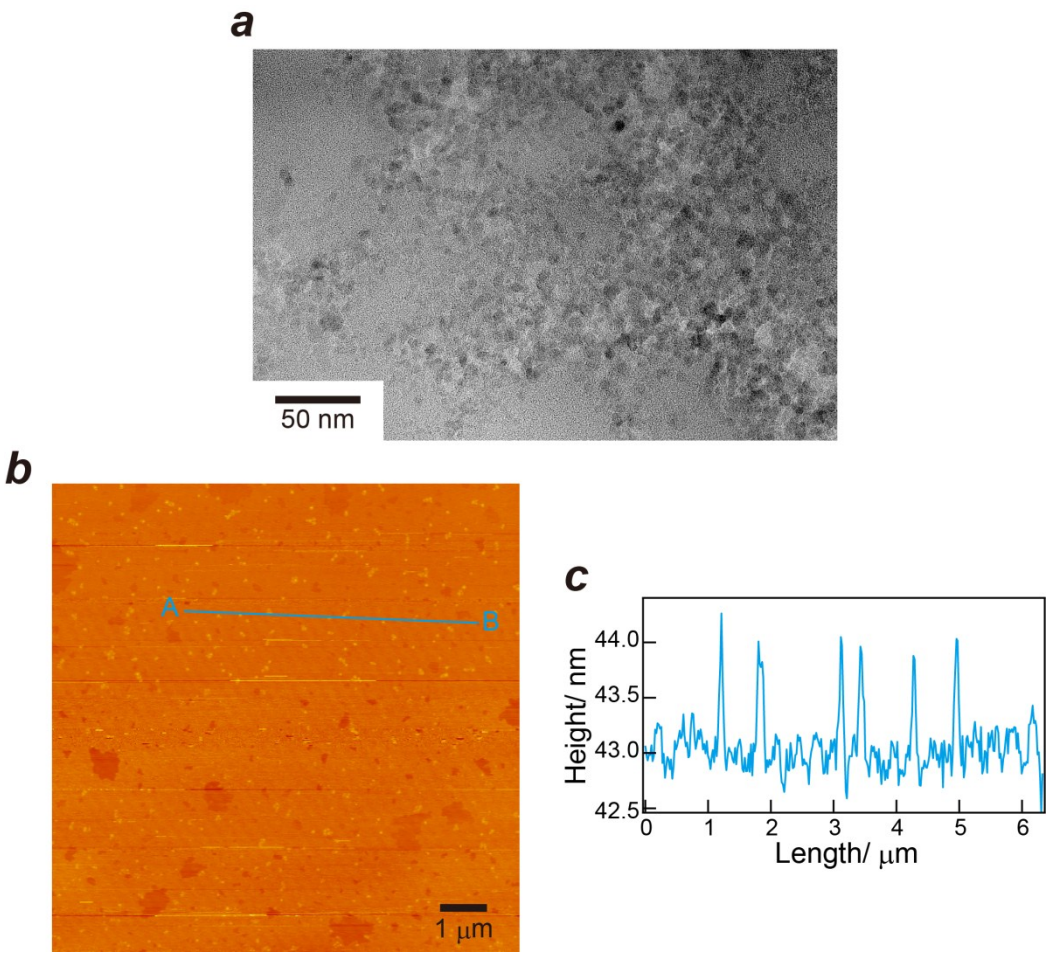

Fig. S2 Characterization of diaminonaphthalene-functionalized graphene quantum dots (DAN-GQDs): (a) TEM image of DAN-GQDs. (b) AFM image of aggregated DAN-GQDs obtained by spin-casting a suspension of the DAN-GQDs in DMF onto mica. (c) Height profile along the line A–B shown in (b).

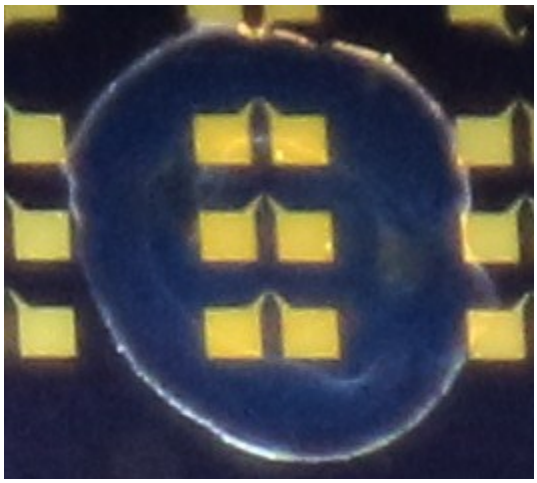

Fig. S3 Optical image of DAN-GQDs/BN-NSs@GFET hybrid photodetector.

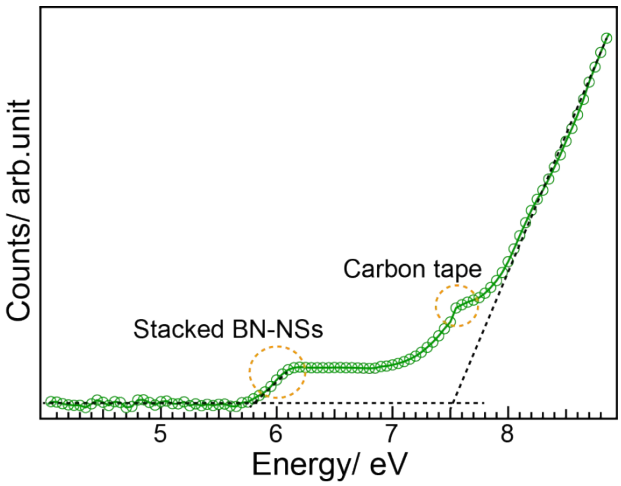

Fig. S4 Photoelectron yield spectra measured for dried BN-NS powder fixed on carbon tape.

Ab initio calculations of defect and impurity states for BN

Calculations of the total energy were conducted using density functional theory (DFT) with plane waves as a basis set and the projector-augmented wave scheme as implemented in the VASP code. The Heyd-Scuseria-Ernzerhof (HSE) hybrid functional was used to accurately calculate the bandgap and the defect formation energies, while the generalized gradient approximation (GGA) usually underestimates the bandgaps of semiconductors. The calculated bandgap of 5.65 eV for h-BN determined using the HSE functional is larger than that with the PBE functional by 1.0 eV, which is consistent with the previous calculation.[1]

Defect formation energies were calculated using the 7×7×1 supercell with 98 atoms separated by a vacuum layer larger than 15 Å to eliminate the interaction between the periodic images. The HSE functional has a large computational cost; therefore, the Γ point was used for Brillouin-zone sampling in the supercell calculations. The errors of k-point sampling were estimated using the PBE functional to be 0.01 and 0.38 eV for neutral and +1 charged carbon impurities at B sites (C_B), respectively.

The defect formation energies $\Delta E^{D,q}(E_F)$, in equilibrium with a N_2 gas phase (N-rich condition) are shown in Fig. S5a. The slopes and kinks of $\Delta E^{D,q}(E_F)$ correspond to the defect charge states and the charge transition levels $\varepsilon(q/q')$, respectively, as summarized in Fig. S5b. The present results are in agreement with the previous calculations for vacancies and carbon substitution.[S1] The results indicate C_B and nitrogen vacancies (V_N) induce the deep levels observed in the CL measurements. The charge transition levels, which are located in the experimentally observed CL spectrum between 3.0 and 4.2 eV are $\varepsilon(+1/0)$ of C_B at 3.6 eV, $\varepsilon(+1/0)$ at 3.3 eV, and $\varepsilon(0/-1)$ at 4.2 eV for N vacancy. $\varepsilon(-2/-3)$ of V_B at 4.3 eV can be identified in the spectrum because of the larger error for the formation energies of largely charged states.

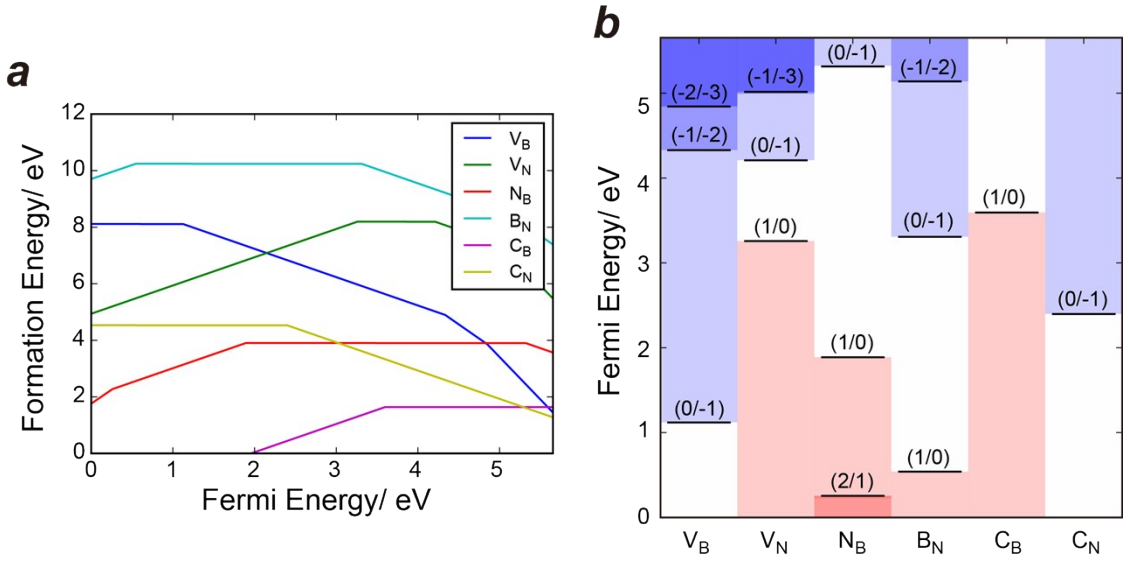

Fig. S5 (a) Calculated formation energies for various models with B or N defects, and B, N or C substitutional impurities: V_B, B defect; V_N, N defect; N_B, substitution of N at a B-site; B_N, substitution of B at an N-site; C_B, substitution of C at a B-site; C_N, substitution of C at an N-site. (b) Summarized charge transition levels.

[S1] B. Huang and H. Lee, *Phys. Rev. B*, 2012, **86**, 245406.

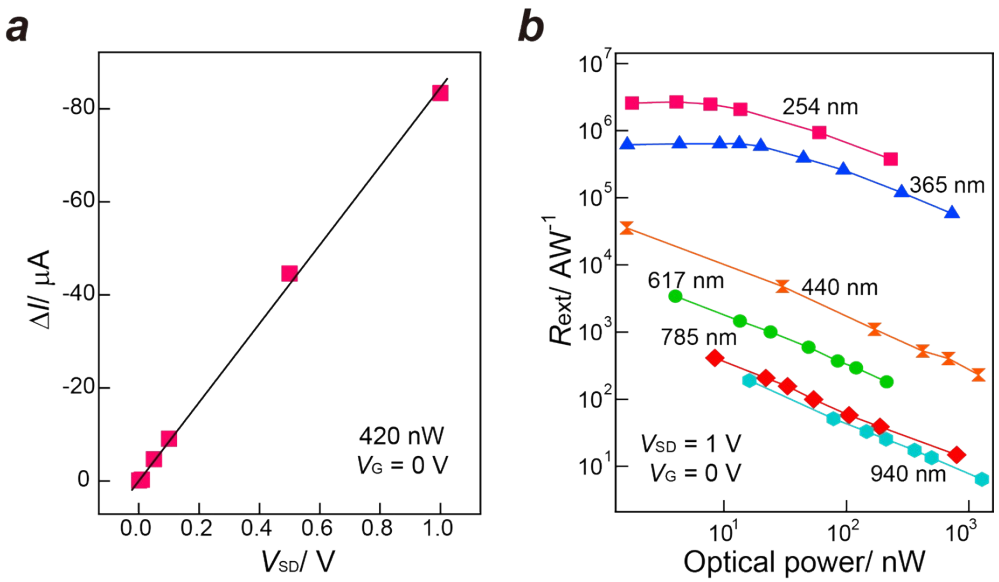

Fig. S6 (a) Source-drain voltage dependency of the photocurrent for the DAN-GQDs/BN-NSs@GFET hybrid photodetector (V_G = 0 V, 440 nm, 420 nW). (b) Photoresponsivity as a function of the optical power for different wavelengths.

Table S1. Summary of the performances of our DAN-GQDs/BN-NSs/graphene hybrid phototransistor and photodetectors of various types, at different wavelengths.

Material	Responsivity (A/W) /Detectivity (Jones)		
	Wavelength		
	UV (<400)	Visible	Infrared (>700)
This work	**~2×10^{6}/~5×10^{13} (254 nm)**	**~2×10^{4}/~8×10^{11} (440 nm)**	**~3×10^{2}/~8×10^{9} (940 nm)**
graphene/ZnO QDs[S2]	~2×10^{7}/~5×10^{13} (335 nm)	~1×10^{4}/~1×10^{11} (500 nm)	-
ZnO NWs[S3]	~1×10^{7}/~8×10^{17} (300 nm)	-	-
Organic-inorganic composites[S4]	~1×10^{3}/~3×10^{15} (360 nm)	-	-
Doped WSe_2[S5]	-	~1×10^{4}/~5×10^{10} (520 nm)	-
Doped MoS_2[S5]	-	~5×10^{3}/~3×10^{8} (520 nm)	-
MoS_2 NSs[S6]	-	~8×10^{2}/~1×10^{7} (561 nm)	-
Mo:$ReSe_2$ NSs[S7]	-	~5×10^{1}/- (633 nm)	-
InSe NSs[S8]	-	~1×10^{1}/~1×10^{11} (450 nm)	~1×10^{0}/- (785 nm)
graphene/PbS QDs[S9]	-	~5×10^{7}/~7×10^{13} (532 nm)	~5×10^{5}/- (1,000 nm)
MoS^2/BP[S10]	-	~2×10^{2}/~3×10^{11} (532 nm)	~0.1/~2×10^{9} (1,550 nm)
Perovskite/Polymer[S11]	~0.01/~6×10^{9} (365 nm)	~0.05/~1×10^{10} (650 nm)	~0.02/~3×10^{9} (835 nm)
Si photodiode	~0.15/~9×10^{11} (300 nm)	~0.3/~1×10^{12} (600 nm)	~0.3/~2×10^{12} (900 nm)

[S2] D. Shao, J. Gao, P. Chow, H. Sun, G. Xin, P. Sharma, J. Lian, N. A. Koratkar, S. Sawyer, *Nano Lett.* 2015, **15**, 3787.

[S3] X. Liu, L. Gu, Q. Zhang, J. Wu, Y.Long, Z. Fan, *Nat. Commun.* 2014, **5**, 4007.

[S4] F. Guo, B. Yang, Y. Yuan, Z. Xiao, Q. Dong, Y. Bi, J. Huang, *Nat. Nanotechnol.* 2012, **7**, 798

[S5] D. Kang, M. Kim, J. Shim, J. Jeon, H. Park, W. Jung, H. Yu, C. Pang, S. Lee, J. Park, *Adv. Funct. Mater.* 2015, **25**, 4219.

[S6] O. Lopez-Sanchez, D. Lembke, M. Kayci, A. Radenovic, A. Kis, *Nat. Nanotechnol.* 2013, **8**, 497.

[S7] S. Yang, S. Tongay, Q. Yue, Y. Li, B. Li, F. Lu, *Sci. Rep.* 2014, **4**, 5442.

[S8] S. R. Tamalampudi, Y. Lu, R. Kumar U., R. Sankar, C. Liao, K. Moorthy B., C. Cheng, F. C. Chou, Y. Chen, *Nano Lett.* 2014, **14**, 2800.

[S9] G. Konstantatos, M. Badioli, L. Gaudreau, J. Osmond, M. Bernechea, F. P. G. Arquer, F. Gatti, F. H. L. Koppens, *Nat. Nanotechnol.* 2012, **7**, 363.

[S10] L. Ye, H. Li, Z. Chen, J. Xu,, *ACS Photon.* 2016, **3**, 692.

[S11] Y. Lee, J. Kwon, E. Hwang, C. Ra, W. J. Yoo, J.-H. Ahn, J. H. Park, J. H. Cho, *Adv. Mater.* 2016, **28**, 5969.

Movie S1. The operation of the infrared photoreflector.